Journal of Cerebral Blood Flow & Metabolism (2011) 31, 1743–1750

www.jcbfm.com

Association between pH-weighted endogenous amide proton chemical exchange saturation transfer MRI and tissue lactic acidosis during acute ischemic stroke

Phillip Zhe Sun[1,2], Jerry S Cheung[1], Enfeng Wang[1] and Eng H Lo[2]

[1]*Department of Radiology, Athinoula A. Martinos Center for Biomedical Imaging, Massachusetts General Hospital and Harvard Medical School, Charlestown, Massachusetts, USA;* [2]*Neuroprotection Research Laboratory, Department of Radiology and Neurology, Massachusetts General Hospital, Harvard Medical School, Charlestown, Massachusetts, USA*

The ischemic tissue becomes acidic after initiation of anaerobic respiration, which may result in impaired tissue metabolism and, ultimately, in severe tissue damage. Although changes in the major cerebral metabolites can be studied using magnetic resonance (MR) spectroscopy (MRS)-based techniques, their spatiotemporal resolution is often not sufficient for routine examination of fast-evolving and heterogeneous acute stroke lesions. Recently, pH-weighted MR imaging (MRI) has been proposed as a means to assess tissue acidosis by probing the pH-dependent chemical exchange of amide protons from endogenous proteins and peptides. In this study, we characterized acute ischemic tissue damage using localized proton MRS and multiparametric imaging techniques that included perfusion, diffusion, pH, and relaxation MRI. Our study showed that pH-weighted MRI can detect ischemic lesions and strongly correlates with tissue lactate content measured by ^{1}H MRS, indicating lactic acidosis. Our results also confirmed the correlation between apparent diffusion coefficient and lactate; however, no significant relationship was found for perfusion, T_1, and T_2. In summary, our study showed that optimized endogenous pH-weighted MRI, by sensitizing to local tissue pH, remains a promising tool for providing a surrogate imaging marker of lactic acidosis and altered tissue metabolism, and augments conventional techniques for stroke diagnosis.
Journal of Cerebral Blood Flow & Metabolism (2011) **31,** 1743–1750; doi:10.1038/jcbfm.2011.23; published online 9 March 2011

Keywords: acute stroke; animal studies; brain ischemia; diffusion-weighted MRI; MRI

Introduction

The cerebral tissue undergoes a complex cascade of metabolic disturbances during acute ischemic stroke—among them are altered glucose and oxygen metabolism, tissue acidosis, adenosine triphosphate depletion, and ultimately, severe tissue damage (An *et al*, 2009; Astrup *et al*, 1981; Hossmann, 1994; Siesjo, 1992*a*). During ischemia, anaerobic respiration is initiated as an alternative to the disrupted oxidative metabolism pathway, which is inefficient for generating high-energy substrates and, because of the production of lactate as a byproduct, often leads to tissue acidosis (Paschen *et al*, 1992). Metabolic disruption may be further exacerbated by hypoperfusion and the reduced buffering capacity of biocarbonate at acidic pH, which may lead to further tissue acidification (Macdonald and Stoodley, 1998; Zauner *et al*, 2002). As sufficient energy metabolism is vital for cell viability and salvageability, it is important to characterize metabolic impairments by monitoring altered energy substrates and lactate concentration, neuronal biomarkers, and tissue pH/acidosis.

Magnetic resonance (MR) techniques including MR imaging (MRI) and MR spectroscopy (MRS) have greatly advanced our understanding of stroke pathophysiology (Guadagno *et al*, 2003; Kloska *et al*, 2010). In particular, perfusion- and diffusion-weighted MRI (PWI and DWI, respectively), two of the most widely used imaging techniques, can quantify tissue hemodynamic and microscopic structural changes.

Correspondence: Dr PZ Sun, Department of Radiology, Athinoula A. Martinos Center for Biomedical Imaging, MGH and Harvard Medical School, 149 13th Street, Room No. 2301, Charlestown, MA 02129, USA.
E-mail: pzhesun@nmr.mgh.harvard.edu
This study was supported in part by grants from AHA/SDG 0835384N, NIH/NIBIB 1K01EB009771-01, NIH/1R21NS061119, and NIH/NCRR-P41RR14075. This work has been presented at the Gordon Research Conference of *in vivo* MR in 2010.
Received 9 October 2010; revised 8 January 2011; accepted 30 January 2011; published online 9 March 2011

In addition, localized MRS (^{1}H and ^{31}P) can detect manifestations of altered tissue metabolism, such as lactate accumulation, glucose, *N*-acetylaspartate (NAA) and adenosine triphosphate depletion, and tissue acidosis. Nevertheless, conventional MR techniques are somewhat limited. In particular, PWI lesions often overestimate infarction volume, whereas early DWI lesions are reversible (Ringer *et al*, 2001). As such, the postulation that a PWI/DWI mismatch approximates the salvageable ischemic penumbra has to be carefully revised (Kidwell *et al*, 2003). Moreover, metabolic derangement in the DWI lesion has been found to be heterogeneous (Guadagno *et al*, 2006; Nicoli *et al*, 2003), although conversely, the sensitivity and spatiotemporal resolution of MRS or spectroscopy imaging are often not sufficient to routinely examine fast-evolving and heterogeneous ischemic lesions. Such limitations underscore the urgency for new techniques to rapidly and specifically demarcate the heterogeneous ischemic tissue's metabolic impairments and to augment conventional MRS/MRI techniques for stroke diagnosis.

As tissue acidosis is associated with anaerobic glycolysis, pH, as measured with biochemical analysis or ^{31}P MRS has been shown as an indicator of altered tissue metabolism and helps to predict tissue outcome (Hata *et al*, 1998; Tomlinson *et al*, 1993). As such, it remains important to develop noninvasive *in vivo* pH MRI techniques to image tissue acidosis. As the chemical exchange between amide protons and bulk tissue water is pH dependent, it has been shown that amide proton chemical exchange saturation transfer (CEST) MRI is capable of assessing tissue pH (Jokivarsi *et al*, 2007; Sun *et al*, 2007*a*; Sun and Sorensen, 2008; Ward and Balaban, 2000; Zhou *et al*, 2003). We have shown that pH-weighted amide proton transfer (APT) MRI is capable of detecting an ischemic lesion, even before diffusion abnormality (Sun *et al*, 2007*b*). In this study, we investigated ischemic tissue damage using multiparametric MRI techniques, including perfusion, diffusion, pH and relaxation MRI, and localized ^{1}H MRS. We evaluated whether pH-weighted MRI can serve as a surrogate metabolic imaging marker for lactic acidosis, complementing commonly used stroke MRI and MRS scans.

Materials and methods

Animal Model

Animal experiments were carried out in accordance with institutional guidelines, as approved by the SRAC, MGH (Subcommittee on Research Animal Care, Massachusetts General Hospital). Adult male Wistar rats ($n = 12$, weighing 312 ± 41 g, Charles River Laboratory, Wilmington, MA, USA) were anesthetized with 1% to 1.5% isoflurane during surgery and MRI. Overall, 2 animals died during the MRI scan and 10 rats ($n = 10$) were included in data analysis. The animal's core temperature was maintained using a circulating warm water jacket positioned around its torso. We induced standard permanent middle cerebral artery occlusion (MCAO) by inserting a 4-0 nylon suture into the lumen of the internal carotid artery to block the origin of the MCA. We also monitored the animal's heart rate and blood oxygen saturation (SpO_2) online during MRI (Nonin Pulse Oximeter 8600; Nonin, Plymouth, MN, USA). In addition, we measured plasma glucose levels immediately before MCAO (Bayer Contour Meter, Tarrytown, NY, USA). Animal body weight, glucose level, typical SpO_2, and heart rate are listed in Table 1.

^{1}H Magnetic Resonance Spectrometry and Magnetic Resonance Imaging

All data were acquired using a standard Bruker cross-coil (volume-coil excitation, surface-coil detection) after high-order Fastmap shimming to achieve a homogeneous magnetic field (B_0 and B_1) and a high signal-to-noise ratio at 4.7 T (Bruker Biospin, Billerica, MA, USA). We obtained *in vivo* MRS using point-resolved single voxel

Table 1 A total of 12 animals received permanent filament MCAO surgery, and scanned for multiparametric MRI and ^{1}H MRS

Animal counts	*Body weight (g)*	*Glucose (mg/dL)*	*SpO_2 (%)*	*Heart rate (beats/min)*	*Inclusion/exclusion*
1	340	—	97	463	+
2	334	—	94	480	+
3	282	148	90	425	+
4	342	179	93	478	+
5	380	158	91	460	+
6	348	161	93	497	+
7	276	136	96	462	+
8	278	150	91	220	Deceased (−)
9	350	179	97	493	Deceased (−)
10	272	158	93	468	+
11	258	133	94	396	+
12	282	179	91	462	+
Mean ± s.d.	312 ± 41	158 ± 17	93 ± 2	442 ± 75	

MCAO, middle cerebral artery occlusion; MRI, magnetic resonance imaging; MRS, magnetic resonance spectroscopy.
The body weight, pre-MCAO plasma glucose level, typical SpO_2, and heart rate of the 12 animals (Nonin Pulse Oximeter 8600) were included herein. Two animals deceased during the MRI scan, and were excluded from data analysis.

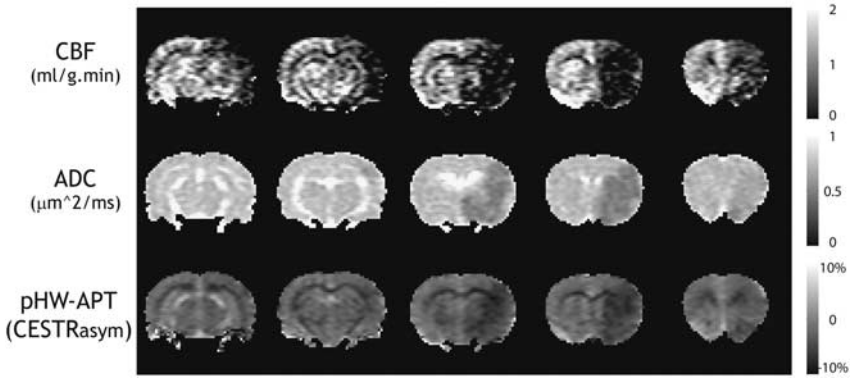

Figure 1 Characterization of ischemic lesion with multiparametric perfusion, diffusion, and pH-weighted APT MRI of a representative acute stroke animal with MCAO. The animal showed a large perfusion and diffusion lesion mismatch, whereas the pH-weighted APT lesion agreed reasonably well with the diffusion deficit. ADC, apparent diffusion coefficient; APT, amide proton transfer; CBF, cerebral blood flow; $CESTR_{asym}$, chemical exchange saturation transfer ratio asymmetry; MCAO, middle cerebral artery occlusion; MRI, magnetic resonance imaging.

spectroscopy from a cubic region of interest of $3.5 \times 3.5 \times 3.5\,mm^3$, positioned approximately in the striatum, which often displays ischemic lesions in the MCAO model; the total acquisition time was ~17 minutes. Multislice MRI (5 slices, slice thickness = 2 mm) was obtained with single-shot echo-planar imaging (field of view: $25 \times 25\,mm^2$, matrix: 64×64, bandwidth: 200 kHz). Gradient-echo readout was used for perfusion, pH-weighted APT, and T_1 MRI (Sun *et al*, 2010*b*), whereas diffusion and T_2 MRI were obtained with spin-echo readout. It is important to note that the gradient-echo echo time (TE) was 14.8 milliseconds, and that the image distortion between the gradient-echo and spin-echo readouts was minimal (Figure 1). In particular, T_1 images were acquired using an inversion recovery sequence, with 7 inversion delays from 250 to 3,000 milliseconds (repetition time (TR)/TE = 6,500/14.8 milliseconds, number of average = 4). T_2 images were obtained with two spin-echo images with TE of 30 and 100 milliseconds (TR = 3,250 milliseconds, number of average = 16). In addition, single-shot isotropic diffusion-weighted MRI was acquired with two *b*-values of 250 and 1,000 seconds/mm^2 (TR/TE = 3,250/54 milliseconds, number of average = 16) (Mori and van Zijl, 1995). Moreover, perfusion imaging was obtained using a continuous arterial spin labeling technique (Alsop and Detre (1998)) (TR/TE = 6,500/14.8 milliseconds, number of average = 32, TS (time of saturation) = 3,250 milliseconds). Finally, for pH-weighted MRI, we set the recovery time to be 5,000 milliseconds, as well as primary radio frequency (RF) saturation duration (TS_1 = 4,500 milliseconds) and secondary RF saturation duration (TS_2 = 500 milliseconds) for an RF irradiation power of 0.75 μT (± 3.5 p.p.m., 700 Hz at 4.7 T) (Sun *et al*, 2010*b*). The control scan was signal averaged 8 times, whereas saturated images were averaged 32 times.

Data Processing

We processed the MRS spectra with Java-based Magnetic Resonance User Interface (jMRUI v4.0, http://www.mrui.uab.es/mrui/), and MRI images with Matlab (Mathworks, Natick, MA, USA). In brief, the raw MRS data were first apodized using a 15-Hz Gaussian filter and phased corrected. Residual water removal was achieved by the Hackel-Lanczos Singular Value Decomposition algorithm (Pijnappel *et al*, 1992). The QUEST (Quantum estimation) method combined with subtraction approach for background modeling was used for measuring metabolite areas. Metabolite model signals of Cho (choline-containing compounds, Cr (total creatine), glutamate/glutamine, NAA, and lactate were quantum mechanically simulated in nuclear magnetic resonance spectra calculation using operators (nuclear magnetic resonance-SCOPE) (Graverondemilly *et al*, 1993). The numerical time-domain model functions of these metabolites were then used as previous knowledge in QUEST. The reliability of metabolite quantitation was assessed by errors in measurements as calculated by the Cramér–Rao lower bounds (Cudalbu *et al*, 2008). In addition, we obtained T_1, T_2, and apparent diffusion coefficient (ADC) maps using least-squares mono-exponential fitting of the signal intensities as a function of inversion time, TE, and *b*-value, respectively. It is important to point out that whereas a mono-exponential decay function seems overly simplistic to describe *in vivo* diffusion, it provides a reasonable delineation of ischemic diffusion lesion and has been widely used in acute ischemic stroke imaging. In addition, a cerebral blood flow (CBF) map was reconstructed using $CBF = \lambda(I_{ref} - I_{label})/(2 \cdot I_{ref} \cdot T_{1sat})$, in which λ is the brain–blood partition coefficient for water (0.63 mL/g) (Alsop and Detre, 1998; Williams *et al*, 1992). We used a representative T_{1sat} of 0.86 seconds, similar to that used by Utting *et al* (2005). The pH-weighted image was derived as CEST ratio asymmetry ($CESTR_{asym}$), which calculates the difference between label and reference images, normalized by the control scan (I_0) per voxel as ($CESTR_{asym} = (I_{ref} - I_{label})/I_0$).

Results

Figure 1 shows CBF, ADC, and pH-weighted APT MR images of a representative acute MCAO animal.

The animal had a reasonably large hypoperfused ischemic lesion spanning all five slices, whereas the diffusion lesion was significantly smaller, covering mainly the third and fourth slices. In comparison, pH-weighted MRI showed an ischemic lesion similar to the diffusion lesion, and significantly smaller than the PWI deficit. As such, there was a sizeable mismatch between the perfusion, pH, and diffusion lesions, indicating the existence of a large viable ischemic tissue shortly after MCAO. In addition, pH-weighted MRI showed different levels of hypointensity, suggesting heterogeneous tissue acidification within PWI and DWI lesions (Bolas *et al*, 1988). It is important to note that whereas Figure 1 shows a reasonably good agreement between pH and diffusion MRI lesion size, we have also observed, in some cases, a sizeable pH and diffusion lesion mismatch. Such findings suggest that the mismatch among perfusion, pH, and diffusion MRI is complex and heterogeneous, and that further study is required to evaluate how pH MRI may augment the commonly used perfusion and diffusion MRI to elucidate ischemic tissue damage (Sun *et al*, 2007*b*).

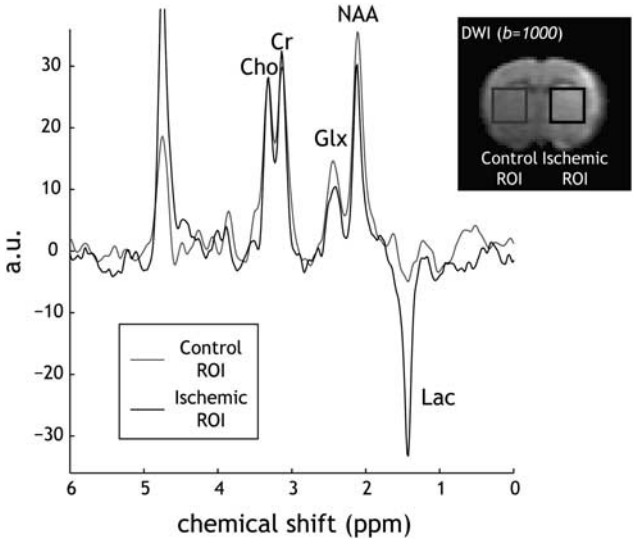

Figure 2 Measurement of ischemic brain metabolites with PRESS MRS. Spectra were acquired (TR/TE = 1,000/144 milliseconds, NA = 1,024) from two ROIs: one in the ipsilateral ischemic lesion, which appeared as hyperintensive in DWI images ($b = 1{,}000\,mm^2$/milliseconds), and the second one chosen in the contralateral normal area to serve as the reference ROI. The displayed spectra were normalized by choline signal, so that change in brain metabolites can be easily realized. Cho, choline-containing compound; Cr, total creatine; DWI, diffusion-weighted imaging; Glx, glutamate/glutamine; MRS, magnetic resonance spectroscopy; NA, number of average; NAA, *N*-acetylaspartate; PRESS, point-resolved single voxel spectroscopy; ROI, region of interest; TE, echo time; TR, repetition time.

Representative localized MRS spectra are shown in Figure 2. Two regions of interest were positioned: one in the striatum, which often displays ischemic abnormality, and the other in the contralateral normal area, approximately symmetric to the ischemic region of interest. To improve the specificity of the lactate MRS signal, we used a long TE of 144 milliseconds, in which the lactate signal is inverted from other metabolite signals, whereas mobile lipid and macromolecular signals are significantly attenuated. Reliable quantitation of various metabolites was indicated by low Cramér–Rao lower bounds, which were calculated to be < 10% in all metabolite estimations (Cudalbu *et al*, 2008). Figure 2 shows that several key metabolites including Cr, Cho, glutamate/glutamine, and NAA can be reasonably detected. It is important to note that choline peaks of the displayed spectra were normalized so that the changes in the spectra could be readily realized (Figure 2). We observed a subtle decrease in NAA signal, consistent with the notion that NAA is an early marker of neuronal damage. Moreover, we observed the inverted lactate signal for the ischemic region of interest, as expected given the chosen TE. The lactate peak was normalized to the sum of creatine and choline (i.e., Lactate/(Cr + Cho)) (Malisza *et al*, 1998), such that the subtle difference between coil loading and the distance between voxel and receiver coil can be normalized (Parsons *et al*, 2000). We also analyzed multiple MRI parameters using a paired two-tailed *t*-test (Table 2).

Table 2 Comparison of multiparametric MRI and ^{1}H MRS measurements during acute ischemic stroke

	Contralateral normal area (mean ± s.d.)	*Ipsilateral ischemic lesion (mean ± s.d.)*	P-*value*
Lactate/(Cho+Cr)	—	0.90 ± 0.35	
NAA/(Cho+Cr)	1.10 ± 0.23	0.79 ± 0.17*	0.012
T_1 (seconds)	1.52 ± 0.07	1.67 ± 0.07*	< 0.0001
T_2 (milliseconds)	55.4 ± 2.2	55.8 ± 2.7	0.45
CBF (mL/g per min)	1.28 ± 0.21	0.53 ± 0.22*	< 0.0001
ADC (μm^2/milliseconds)	0.76 ± 0.01	0.59 ± 0.07*	< 0.0001
$CESTR_{asym}$ (%)	−3.8 ± 0.7	−5.9 ± 0.7*	< 0.0001
$CESTR_{asym}/T_1$ (%)	−2.5 ± 0.5	−3.5 ± 0.5*	< 0.0001

ADC, apparent diffusion coefficient; CBF, cerebral blood flow; $CESTR_{asym}$, chemical exchange saturation transfer ratio asymmetry; Cho, choline-containing compound; Cr, total creatine; MRI, magnetic resonance imaging; MRS, magnetic resonance spectroscopy; NAA, *N*-acetylaspartate.
Ischemic lesions showed significant changes in T_1, CBF, ADC, and pH-weighted amide proton $CEST_{asym}$ and the normalized NAA content, whereas no significant T_2 change was observed.
*$P < 0.05$.

In particular, the mean CBF decreased from 1.28 ± 0.21 mL/g per min to 0.53 ± 0.22 mL/g per min ($P < 0.0001$), and ADC decreased from $0.76 \pm 0.01\ \mu m^2$/milliseconds to $0.59 \pm 0.07\ \mu m^2$/milliseconds ($P < 0.0001$). In addition, pH-weighted $CESTR_{asym}$ decreased from $-3.8\% \pm 0.7\%$ to $-5.9\% \pm 0.7\%$ ($P < 0.0001$). T_1 increased slightly from 1.52 ± 0.07 seconds to 1.67 ± 0.07 seconds ($P < 0.0001$), consistent with the observation made by Kaur *et al* (2009). Conversely, we observed no significant change in T_2, which we measured at 55.4 ± 2.2 milliseconds and at 55.8 ± 2.7 milliseconds, respectively ($P > 0.05$).

We evaluated the association between MRI and normalized lactate content (i.e., Lactate/(Cr + Cho)) with linear regression (Figure 3). No significant correlation was found between T_1 ($R^2 = 0.21$, significance F = 0.18) and T_2 ($R^2 = 0.01$, significance F = 0.75). In addition, the correlation between CBF and lactate was not significant ($R^2 = 0.03$, significance F = 0.61). Importantly, ADC ($R^2 = 0.50$, significance F = 0.02) and pH-weighted $CESTR_{asym}$ ($R^2 = 0.55$, significance F = 0.01) significantly correlated with lactate content, indicating that the severity of diffusion reduction and tissue acidosis is associated with lactate (Cvoro *et al*, 2009).

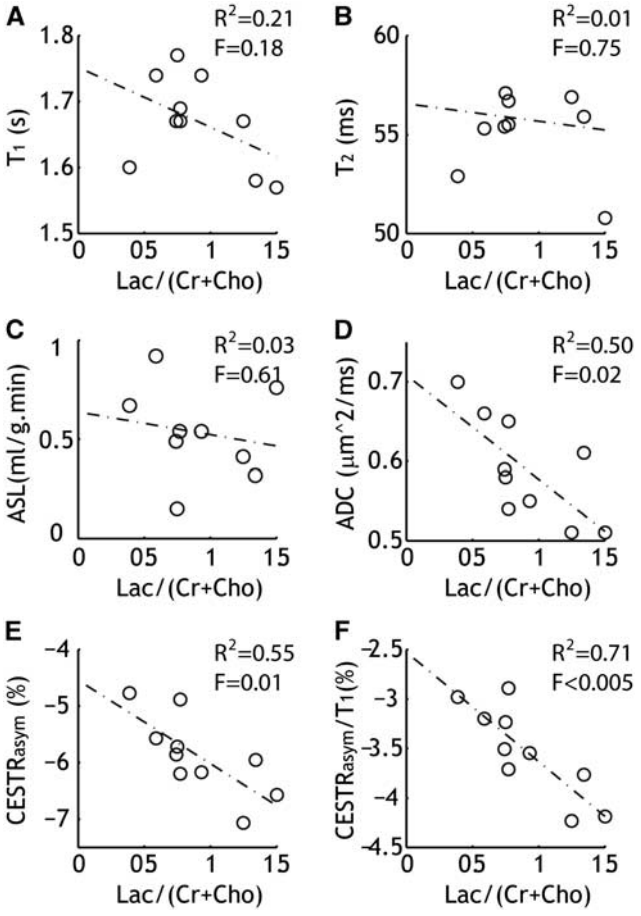

Figure 3 Association between MRS measurement of brain lactate content and multiple MRI parameters ($n = 10$). Linear regression test showed a significant correlation between ADC (**D**), pH-weighted APT MRI (**E**), and T_1-normalized APT MRI (**F**) with normalized lactate content (Lac/(Cho + Cr)), whereas no such relationship was found for CBF (**A**) and relaxation measurements (**B, C**). ADC, apparent diffusion coefficient; APT, amide proton transfer; ASL, arterial spin labeling; CBF, cerebral blood flow; $CESTR_{asym}$, chemical exchange saturation transfer ratio asymmetry; Cho, choline-containing compound; Cr, total creatine; MRI, magnetic resonance imaging; MRS, magnetic resonance spectroscopy.

Moreover, given that CEST contrast scales approximately with T_1, T_1-normalized CEST contrast should more faithfully capture the pH-induced contrast. In particular, CEST contrast can be described as $\mathrm{CESTR} = \frac{f \cdot k_{sw}}{R_{1w} + f \cdot k_{sw}} \cdot \alpha \cdot (1 - \sigma)$, where k_{sw} is amide proton chemical exchange rate, f the amide proton concentration with regard to bulk water proton, R_{1w} the bulk water longitudinal relaxation rate, α is labeling coefficient, and σ the spillover factor (Sun *et al*, 2005). Owing to the fact that endogenous amide proton concentration is relatively dilute and the exchange rate is relatively slow, we have $f \cdot k_{sw}(\mathrm{pH}) \approx \frac{\mathrm{CESTR}}{1 - \mathrm{CESTR}} \cdot \frac{1}{T_{1w}} \approx \frac{\mathrm{CESTR}}{T_{1w}}$ (Sun and Sorensen, 2008). As such, it is not surprising that the correlation between pH-weighted MRI and lactate was significantly improved when the T_1 effect was taken into account (i.e., $CESTR_{asym}/T_1$), calculated as $R^2 = 0.71$ and significance F < 0.005.

Discussion

Our study showed that T_1-normalized pH-weighted APT/CEST MRI is capable of detecting ischemic lactic acidosis, consistent with previous findings (Jokivarsi *et al*, 2007; Katsura *et al*, 1991). In this study, we assessed lactic acidosis with an emerging endogenous pH-weighted MRI technique, the sensitivity and spatiotemporal resolution of which are significantly higher than those of conventional, ^{1}H and ^{31}P spectroscopy. Whereas it has been suggested that endogenous APT MRI contrast mainly reflects intracellular compartment because of its high concentration of mobile proteins/peptides in the cytoplasm (Zhou *et al*, 2003), Kintner *et al* (1999) showed that intracellular pH and extracellular pH quickly equilibrate after an initial brief buffering phase that delays the sudden change in intracellular pH. Therefore, it seems reasonable to assume that for the case of ischemic stroke, endogenous APT MRI should reflect local tissue pH. Indeed, our previous study has shown that there may be a sizeable CBF/pH/ADC mismatch in acute ischemic stroke animals, and that pH-weighted APT lesions can better predict tissue outcome (Sun *et al*, 2007*b*). In that study, we also postulated that pH-weighted MRI may help delineate the PWI/DWI mismatch into a benign oligemic region and metabolic penumbra, and thereby augment the commonly used PWI/DWI stroke MRI. As such, it remains interesting to further develop pH MRI as a surrogate imaging marker of impaired tissue metabolism and translate pH-weighted APT MRI to the

clinic for investigation of patients with acute stroke (Sun *et al*, 2008, 2010*a*; Zhou *et al*, 2003). Towards this goal, we have recently proposed an unevenly segmented RF irradiation scheme, which enables multislice acquisition with improved sensitivity (Sun *et al*, 2010*b*). Such work should facilitate the validation of *in vivo* pH-weighted MRI, so that it may help delineate heterogeneous ischemic tissue damage based on the hemodynamic, metabolic, and structural status of the tissue, as estimated with multiparametric MRI and MRS, with the ultimate goal to guide individualized stroke treatment (Jacobs *et al*, 2000; Shen *et al*, 2005; Wu *et al*, 2001).

Whereas tissue pH correlates with lactate during acute ischemia, their relationship is complex upon reperfusion or for prolonged ischemia. For instance, pH may recover despite significantly elevated lactate, likely facilitated by alternative acid extrusion mechanisms (Allen *et al*, 1988; Pirttilä and Kauppinen, 1992). As such, it is important to monitor multiple parameters to better assess ischemic tissue metabolism for predicting tissue outcome and response to potential treatments, particularly in cases with significant residual/collateral flow or autolysis, towards which an imaging-based sensitive pH MRI technique is helpful. Nevertheless, commonly used *in vivo* APT MRI is somewhat oversimplified, and provides only pH-weighted information. Notably, the CEST asymmetry analysis is susceptible to concomitant RF irradiation effects, particularly, the slightly asymmetric magnetization transfer and nuclear overhauser effect (Pekar *et al*, 1996). For instance, there is a subtle baseline shift between the white matter and the gray matter in the brain $CEST_{asym}$ map (Figure 1). Fortunately, magnetization transfer and nuclear overhauser effect contrasts show little change with pH during acute ischemia, and thereby they only induce an asymmetry shift and the *in vivo* APT/CEST asymmetry analysis still provides pH-weighted contrast (Chen *et al*, 2006; Makela *et al*, 2002). In addition, confounding factors such as tissue temperature, edema, and relaxation time change may also affect the experimentally obtained pH MRI contrast. However, cerebral temperature change during focal ischemia is relatively small. In addition, the exchange rate decreases at lower temperature, which should enhance pH-weighted MRI contrast, and so does edema. Moreover, edema and T_1 increase should partially offset the effects of each. This agrees with our finding that T_1-normalized endogenous CEST asymmetry analysis provides stronger correlation with lactate content than that without T_1 normalization. Nevertheless, additional work is urgently required to enhance the pH specificity of *in vivo* pH-weighted MRI and, ultimately, to develop quantitative tissue pH imaging.

Our study also measured plasma glucose levels immediately before filament occlusion, being 157 ± 17 mg/dL ($n = 8$). However, no significant correlation was found between preischemic glucose levels and lactate content after occlusion ($R^2 = 0.11$, significance $F = 0.43$). This suggested that confounding factors other than the preischemic glucose level may also affect lactic acidosis, for instance, collateral flow, oxygen delivery/consumption, and potentially the variance of MCAO model. In addition, the range of plasma glucose level was relatively narrow because of the use of young healthy animals, making it somewhat difficult to investigate the preischemic glucose effect on lactate and tissue acidification. Whereas conversely, it is expected that lactate levels will be elevated in cases of severe hyperglycemia such as diabetes mellitus, a disease for which it will be very interesting to test whether pH MRI can assess lactic acidosis and relevant pathophysiological changes (Parsons *et al*, 2002). In fact, it has been shown that preischemic hyperglycemia aggravates ischemic tissue damage, likely owing to worsened tissue acidosis (Siesjo, 1992*b*). As such, it is vitally important to elucidate the relationship between metabolic disruption, lactate, acidosis, and tissue damage. Finally, whereas our current study used a permanent stroke model to elucidate the correlation between tissue pH, diffusion, and lactic acidosis, it remains very promising to extend pH MRI to applications such as transient ischemic attack and cortical spreading depression in which the tissue pH change is dynamic and heterogeneous (Bisschops *et al*, 2002; Mutch and Hansen, 1984; Sukhotinsky *et al*, 2008).

Conclusions

Our study characterized heterogeneous ischemic tissue damage with multiparametric MRI of perfusion, pH, diffusion and relaxation imaging, and localized ^{1}H MRS. We showed that T_1-compensated pH-weighted endogenous amide proton CEST and diffusion MRI significantly correlated with lactate content, whereas no such correlation was found for perfusion and relaxation MRI. As such, our data show that pH-weighted MRI, by sensitizing to tissue acidification, provides a surrogate imaging marker of lactic acidosis and disrupted tissue metabolism, aiding the widely used MRI and MRS techniques for charactering heterogeneous ischemic tissue damage.

Acknowledgements

The authors thank Dr Risto Kauppinen for helpful discussion.

Disclosure/conflict of interest

The authors declare no conflict of interest.

References

Allen K, Busza AL, Crockard HA, Frackowiak RSJ, Gadian DG, Proctor E, Ross Russell RW, Williams SR (1988) Acute Cerebral Ischaemia: Concurrent Changes in Cerebral Blood Flow, Energy Metabolites, pH, and Lactate Measured with Hydrogen Clearance and 31P and1H Nuclear Magnetic Resonance Spectroscopy. III. Changes Following Ischaemia. *J Cereb Blood Flow Metab* 8:816–21

Alsop DC, Detre JA (1998) Multisection cerebral blood flow MR imaging with continuous arterial spin labeling. *Radiology* 208:410–6

An H, Liu Q, Chen Y, Lin W (2009) Evaluation of MR-Derived Cerebral Oxygen Metabolic Index in Experimental Hyperoxic Hypercapnia, Hypoxia, and Ischemia. *Stroke* 40:2165–72

Astrup J, Siesjo BK, Symon L (1981) Thresholds in cerebral ischemia—the ischemic penumbra. *Stroke* 12: 723–5

Bisschops RHC, Kappelle LJ, Mali WPTM, van der Grond J (2002) Hemodynamic and Metabolic Changes in Transient Ischemic Attack Patients: A Magnetic Resonance Angiography and 1H-Magnetic Resonance Spectroscopy Study Performed Within 3 Days of Onset of a Transient Ischemic Attack. *Stroke* 33:110–5

Bolas NM, Rajagopalan B, Mitsumori F, Radda GK (1988) Metabolic changes during experimental cerebral ischemia in hyperglycemic rats, observed by 31P and 1H magnetic resonance spectroscopy. *Stroke* 19:608–14

Chen JH, Sambol EB, DeCarolis P, O'Connor R, Geha RC, Wu YV, Singer S (2006) High-resolution MAS NMR spectroscopy detection of the spin magnetization exchange by cross-relaxation and chemical exchange in intact cell lines and human tissue specimens. *Magn Reson Med* 55:1246–56

Cudalbu C, Cavassila S, Rabeson H, van Ormondt D, Graveron-Demilly D (2008) Influence of measured and simulated basis sets on metabolite concentration estimates. *NMR Biomed* 21:627–36

Cvoro V, Wardlaw JM, Marshall I, Armitage PA, Rivers CS, Bastin ME, Carpenter TK, Wartolowska K, Farrall AJ, Dennis MS (2009) Associations Between Diffusion and Perfusion Parameters, N-Acetyl Aspartate, and Lactate in Acute Ischemic Stroke. *Stroke* 40:767–72

Graverondemilly D, Diop A, Briguet A, Fenet B (1993) Product-Operator Algebra for Strongly Coupled Spin Systems. *J Magn Reson, Series A* 101:233–9

Guadagno JV, Calautti C, Baron JC (2003) Progress in imaging stroke: emerging clinical applications. *Br Med Bull* 65:145–57

Guadagno JV, Jones PS, Fryer TD, Barret O, Aigbirhio FI, Carpenter TA, Price CJ, Gillard JH, Warburton EA, Baron J-C (2006) Local Relationships Between Restricted Water Diffusion and Oxygen Consumption in the Ischemic Human Brain. *Stroke* 37:1741–8

Hata R, Mies G, Wiessner C, Fritze K, Hesselbarth D, Brinker G, Hossmann K-A (1998) A Reproducible Model of Middle Cerebral Artery Occlusion in Mice: Hemodynamic, Biochemical, and Magnetic Resonance Imaging. *J Cereb Blood Flow Metab* 18:367–75

Hossmann KA (1994) Viability thresholds and the penumbra of focal ischemia. *Ann Neurol* 36:557–65

Jacobs MA, Knight RA, Knight HS-Z, Zhang GZ, Goussev AV, Peck DJ, Windham JP, Chopp M (2000) Unsupervised segmentation of multiparameter MRI in experimental cerebral ischemia with comparison to T2, diffusion, and ADC MRI parameters and histopathological validation. *Stroke* 11:425–37

Jokivarsi KT, Gröhn HI, Gröhn OH, Kauppinen RA (2007) Proton transfer ratio, lactate, and intracellular pH in acute cerebral ischemia. *Magn Reson Med* 57: 647–53

Katsura K, Ekholm A, Anders B, Siesjo BK (1991) Extracellular pH in the Brain During Ischemia: Relationship to the Severity of Lactic Acidosis. *J Cereb Blood Flow Metab* 11:597–9

Kaur J, Tuor UI, Zhao Z, Petersen J, Jin AY, Barber PA (2009) Quantified T1 as an adjunct to apparent diffusion coefficient for early infarct detection: a high-field magnetic resonance study in a rat stroke model. *Int J Stroke* 4:159–68

Kidwell CS, Alger JR, Saver JL (2003) Beyond mismatch: evolving paradigms in imaging the ischemic penumbra with multimodal magnetic resonance imaging. *Stroke* 34:2729–35

Kintner DB, Anderson ME, Sailor KA, Dienel G, Fitzpatrick Jr JH, Gilboe DD (1999) *In vivo* microdialysis of 2-deoxyglucose 6-phosphate into brain: a novel method for the measurement of interstitial pH using ^{31}P-NMR. *J Neurochem* 72:405–12

Kloska SP, Wintermark M, Engelhorn T, Fiebach JB (2010) Acute stroke magnetic resonance imaging: current status and future perspective. *Neuroradiology* 52: 189–201

Macdonald R, Stoodley M (1998) Pathophysiology of cerebral ischemia. *Neurol Med Chir (Tokyo)* 38:1–11

Makela HI, Kettunen MI, Grohn OH, Kauppinen RA (2002) Quantitative $T_{1\rho}$ and magnetic transfer magnetic resonance imaging of acute cerebral ischemia in the rat. *J Cereb Blood Flow Metab* 22:547–58

Malisza K, Kozlowski P, Peeling J (1998) A review of *in vivo* 1H magnetic resonance spectroscopy of cerebral ischemia in rats. *Biochem Cell Biol* 76:487–96

Mori S, van Zijl PCM (1995) Diffusion weighting by the trace of the diffusion tensor within a single scan. *Magn Reson Med* 33:41–52

Mutch WAC, Hansen AJ (1984) Extracellular pH Changes During Spreading Depression and Cerebral Ischemia: Mechanisms of Brain pH Regulation. *J Cereb Blood Flow Metab* 4:17–27

Nicoli F, Lefur Y, Denis B, Ranjeva JP, Confort-Gouny S, Cozzone PJ (2003) Metabolic Counterpart of Decreased Apparent Diffusion Coefficient During Hyperacute Ischemic Stroke: A Brain Proton Magnetic Resonance Spectroscopic Imaging Study. *Stroke* 34:82–7

Parsons MW, Barber PA, Desmond PM, Baird TA, Darby DG, Byrnes G, Tress BM, Davis SM (2002) Acute hyperglycemia adversely affects stroke outcome: a magnetic resonance imaging and spectroscopy study. *Ann Neurol* 52:20–8

Parsons MW, Li T, Barber PA, Yang Q, Darby DG, Desmond PM, Gerraty RP, Tress BM, Davis SM (2000) Combined 1H MR spectroscopy and diffusion-weighted MRI improves the prediction of stroke outcome. *Neurology* 55:498–506

Paschen W, Mies G, Hossmann KA (1992) Threshold relationship between cerebral blood flow, glucose utilization, and energy metabolites during development of stroke in gerbils. *Exp Neurol* 117:325–33

Pekar J, Jezzard P, Roberts DA, Leigh JS, Frank JA, Mclaughlin AC (1996) Perfusion imaging with compensation for asymmetric magnetization transfer effects. *Magn Reson Med* 35:70–9

Pijnappel WWF, van den Boogaart A, de Beer R, van Ormondt D (1992) SVD-based quantification of magnetic resonance signals. *J Magn Reson, Series A* 97:122–34

Pirttilä TRM, Kauppinen RA (1992) Recovery of intracellular pH in cortical brain slices following anoxia studied by nuclear magnetic resonance spectroscopy: Role of lactate removal, extracellular sodium and sodium/hydrogen exchange. *Neuroscience* 47:155–64

Ringer TM, Neumann-Haefelin T, Sobel RA, Moseley ME, Yenari MA (2001) Reversal of early diffusion-weighted magnetic resonance imaging abnormalities does not necessarily reflect tissue salvage in experimental cerebral ischemia. *Stroke* 32:2362–9

Shen Q, Ren H, Fisher M, Duong TQ (2005) Statistical prediction of tissue fate in acute ischemic brain injury. *J Cereb Blood Flow Metab* 25:1336–45

Siesjo BK (1992*a*) Pathophysiology and treatment of focal cerebral ischemia: Part I: Pathophysiology. *J Neurosurg* 77:169–84

Siesjo BK (1992*b*) Pathophysiology and treatment of focal cerebral ischemia: Part II: Mechanisms of damage and treatment. *J Neurosurg* 77:337–54

Sukhotinsky I, Dilekoz E, Moskowitz MA, Ayata C (2008) Hypoxia and hypotension transform the blood flow response to cortical spreading depression from hyperemia into hypoperfusion in the rat. *J Cereb Blood Flow Metab* 28:1369–76

Sun PZ, Benner T, Copen W, Sorensen A (2010*a*) Early experience of translating pH-weighted MRI to image human subjects at 3 Tesla. *Stroke* 41:S147–51

Sun PZ, Benner T, Kumar A, Sorensen AG (2008) Investigation of optimizing and translating pH-sensitive pulsed-chemical exchange saturation transfer (CEST) imaging to a 3T clinical scanner. *Magn Reson Med* 60:834–41

Sun PZ, Cheung JS, Wang E, Benner T, Sorensen AG (2010*b*) Fast multi-slice pH-weighted chemical exchange saturation transfer (CEST) MRI with unevenly segmented RF irradiation. *Magn Reson Med* 64:588–94

Sun PZ, Sorensen AG (2008) Imaging pH using the Chemical Exchange Saturation Transfer (CEST) MRI: Correction of Concomitant RF Irradiation Effects to Quantify CEST MRI for Chemical Exchange Rate and pH. *Magn Reson Med* 60:390–7

Sun PZ, van Zijl PCM, Zhou J (2005) Optimization of the irradiation power in chemical exchange dependent saturation transfer experiments. *J Magn Reson* 175: 193–200

Sun PZ, Zhou J, Huang J, van Zijl P (2007*a*) Simplified Quantitative Description of Amide Proton Transfer (APT) Imaging During Acute Ischemia. *Magn Reson Med* 57:405–10

Sun PZ, Zhou J, Sun W, Huang J, van Zijl PC (2007*b*) Detection of the ischemic penumbra using pH-weighted MRI. *J Cereb Blood Flow Metab* 27:1129–36

Tomlinson FH, Anderson RE, Meyer FB (1993) Acidic foci within the ischemic penumbra of the New Zealand white rabbit. *Stroke* 24:2030–9

Utting JF, Thomas DL, Gadian DG, Helliar RW, Lythgoe MF, Ordidge RJ (2005) Understanding and optimizing the amplitude modulated control for multiple-slice continuous arterial spin labeling. *Magn Reson Med* 54: 594–604

Ward KM, Balaban RS (2000) Determination of pH using water protons and chemical exchange dependent saturation transfer (CEST). *Magn Reson Med* 44:799–802

Williams D, Detre J, Leigh J, Koretsky A (1992) Magnetic resonance imaging of perfusion using spin inversion of arterial water. *Proc Natl Acad Sci* 89:212–6

Wu O, Koroshetz WJ, Ostergaard L, Buonanno FS, Copen WA, Gonzalez RG, Rordorf G, Rosen BR, Schwamm LH, Weisskoff RM, Sorensen AG (2001) Predicting Tissue Outcome in Acute Human Cerebral Ischemia Using Combined Diffusion- and Perfusion-Weighted MR Imaging. *Stroke* 32:933–42

Zauner A, Daugherty W, Bullock M, Warner D (2002) Brain oxygenation and energy metabolism: part I-biological function and pathophysiology. *Neurosurg* 51:289–301

Zhou J, Payen JF, Wilson DA, Traystman RJ, van Zijl PC (2003) Using the amide proton signals of intracellular proteins and peptides to detect pH effects in MRI. *Nat Med* 9:1085–90